# Conformal metasurfaces synthesis in the sense of distribution

N. Lebbe* and S. Lanteri
*Université Côte d'Azur, Inria, CNRS, LJAD, 06902 Sophia Antipolis Cedex, France*

S. Y. Golla and P. Genevet
*Université Cote d'Azur, CNRS, CRHEA, Rue Bernard Gregory, Sophia Antipolis, 06560 Valbonne, France*
(Dated: September 3, 2021)

Visual perception relies on light scattering at the object's surface in the direction of observation. By engineering the surface scattering properties, it is possible to realize arbitrary visual percept. Here, we address theoretically this problem of electromagnetic field transition conditions at conformal interfaces to achieve surface topography-dependent transmitted and reflected fields. Our analysis, supported by two- and three-dimensional finite element simulations, provides a solid theoretical framework to design metasurfaces for cloaking, wearable optics and next generation of freeform imaging systems.

## I. INTRODUCTION

For centuries, optical design consisted in developing thin films and various coating to address light reflection, transmission and/or diffusion at interfaces. Developments in nanophotonics have strongly improved our ability to control light scattering processes with optically resonant nanostructures. Artificial optical materials, also dubbed metamaterials and metasurfaces, presenting unexpected light propagation effects have been realized, leading to cloacking [1], negative refraction [2, 3], subwavelength focusing, generalized refraction [4] and vectorial electromagnetic field control [5–8]. Today these "conventional" metamaterials and metasurfaces are realized assembling subwavelength photonic structures. The study of the device's optical response is generally complex and requires lengthy numerical simulations that describe in detail the effect of light interaction with a large number of nanophotonic building blocks. To avoid modelling thousands and billions of small geometric features, homogenisation methods that approximate the complexity of an inhomogeneous material filed with nanoscale inclusions by its effective medium response, i.e. homogeneous artificial material, have been proposed [9, 10]. For the case of metasurfaces, consisting of a surfacic two-dimensional arrangement of nanostructures, equivalent transition conditions linking the values of the macroscopic field quantities on both sides of a thin homogenized layer have been derived. In fact, such transition conditions are well known in electromagnetics but also in acoustics and are commonly used to simplify physical interpretation or ease numerical simulations [11–13]. Metasurfaces have thus been modelled using advanced effective transition conditions, called Generalized Sheet Transition Conditions (GSTCs). GSTCs were originally derived in optics in the 90s in the seminal paper of Idemen [14]. These transition conditions conceal in a tensorial form the equivalent response occurring on reflecting and transmitting fields at complex interfaces. Efforts to reproduce above-mentioned intriguing effects using GSTC formulation, including anomalous refraction, cloaking and vectorial electromagnetic field control have been realized recently [15, 16]. But so far, modelling relied on Idemen's original work, and most papers dealing with GSTCs only considered layers manufactured on planar surfaces.

Here, we provide a fully self-contained introduction to GSTCs on arbitrary geometries - namely conformal GSTCs (C-GSTCs) - with all the necessary theoretical and numerical tools to exploit these transition conditions. A schematic of the studied problem is presented in Fig. 1). Inspired by Idemen's original idea to calculate the reflection and transmission properties of field discontinuity at planar interfaces, our derivation considers both electric and magnetic surface distributions on a shaped surface (see formal description in the appendices). We express these quantities in the sense of the distribution function along the surface. After deriving the C-GSTCs, we explain the inversion procedure to synthesize the susceptibilities of conformal interfaces for arbitrary input-output fields. Finally, a numerical implementation of these expressions using a finite element method (FEM) is realized to study the angular sensitivity of simple metasurfaces, including deflector and lenses, and we also propose a generic method for surface cloaking of complex objects.

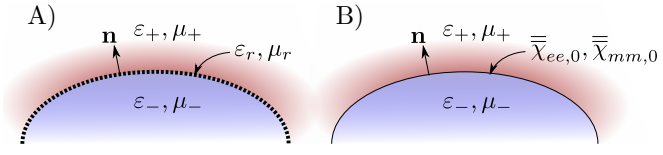


FIG. 1. Schematic representation of conformal metasurfaces. A) light reflection and refraction across a conformal metasurface defined by an ensemble of nanostructured materials along the curved surface; B) The conformal metasurface is modelled using equivalent GSTCs and the associated physical properties defined along the surface to satisfy the input-output field discontinuities.

* Corresponding author: lebbe.nicolas@gmail.com

## II. DERIVATION OF CONFORMAL GSTCS USING SURFACIC DISTRIBUTIONS

We consider Maxwell's equations in the time-harmonic regime assuming a time-dependency in $\exp(+i\omega t)$:

$$\nabla\times\mathbf{E}=-i\omega\mathbf{B},\quad \nabla\times\mathbf{H}=i\omega\mathbf{D},\quad \nabla\cdot\mathbf{D}=0,\quad \nabla\cdot\mathbf{B}=0. \quad (1)$$

together with the following (simply anisotropic) constitutive relations linking the electromagnetic fields with the electric and magnetic inductions through electric and magnetic susceptibility tensors:

$$\mathbf{D}=\varepsilon_0(\overline{\overline{\chi}}_{ee}+1)\mathbf{E}\quad\text{and}\quad\mathbf{B}=\mu_0(\overline{\overline{\chi}}_{mm}+1)\mathbf{H}. \quad (2)$$

With these definitions, the electromagnetic fields satisfies the following natural transition conditions at the interface between two media:

$$\boldsymbol{n}\times[\![\mathbf{E}]\!]=\mathbf{0},\quad \boldsymbol{n}\times[\![\mathbf{H}]\!]=\mathbf{0},\quad \boldsymbol{n}\cdot[\![\mathbf{D}]\!]=0,\quad \boldsymbol{n}\cdot[\![\mathbf{B}]\!]=0,$$

With a metasurface however, the interface is covered with resonant nanostructures of various geometries that can resonatly interact with the incident light, inducing localized surface electric and magnetic dipole moments at the interface plane responsible for electromagnetic field discontinuities. This interaction modifies the natural transition conditions. The derivation of C-GSTCs begin by considering that discontinuities may be formally treated by decomposing the fields ($\mathbf{A}=\mathbf{E},\mathbf{H},\mathbf{D},\mathbf{B}$) according to a series of $n$-th derivatives of Dirac delta functions $\delta_S^{(n)}$ defined along the surface (a proper mathematical definition of this distribution is provided in appendix II). We consider here an arbitrary conformal metasurface located on a two-dimensional surface $S=\{(x,y,z),z=f(x,y)\}$, as presented in Fig. 1, and assume that each field $\mathbf{A}$ can be decomposed as a series of Dirac's surface distribution $\delta_S$ with multiple singular and one regular part as follows:

$$\mathbf{A}(\boldsymbol{x})=\overline{\mathbf{A}}(\boldsymbol{x})+\sum_{n=0}^{\infty}\mathbf{A}_n(x,y)\delta_S^{(n)}(\boldsymbol{x}), \quad (3)$$

where the $\mathbf{A}_n$ are the singular parts of $\mathbf{A}$ defined on the conformal interface while the regular part $\overline{\mathbf{A}}$ is given by:

$$\overline{\mathbf{A}}(\boldsymbol{x})=\mathbf{A}_+(\boldsymbol{x})\text{ if }z>f(x,y)\text{ and }\mathbf{A}_-(\boldsymbol{x})\text{ if }z<f(x,y).$$

Now and for the remainder of this paper, we will consider that $\mathbf{A}_n=0$ for $n>0$ (this is due to the fact that we are only interested in the first order transition conditions verified by the fields). By substituting the distribution form of the fields from (3) into Maxwell equations (1) and using the identities discussed in appendix II, which provides the curl and divergence of singular fields, we then find that:

$$(\nabla_\parallel\times\mathbf{E}_0)\delta_S+\boldsymbol{n}\times\mathbf{E}_0\partial_{\boldsymbol{n}}\delta_S+\overline{\nabla\times\mathbf{E}}+\boldsymbol{n}\times[\![\mathbf{E}]\!]\,\delta_S=-i\omega\left(\mathbf{B}_0\delta_S+\overline{\mathbf{B}}\right), \quad (4)$$

$$(\nabla_\parallel\times\mathbf{H}_0)\delta_S+\boldsymbol{n}\times\mathbf{H}_0\partial_{\boldsymbol{n}}\delta_S+\overline{\nabla\times\mathbf{H}}+\boldsymbol{n}\times[\![\mathbf{H}]\!]\,\delta_S=i\omega\left(\mathbf{D}_0\delta_S+\overline{\mathbf{D}}\right), \quad (5)$$

$$(\nabla_\parallel\cdot\mathbf{D}_0)\delta_S+\boldsymbol{n}\cdot\mathbf{D}_0\partial_{\boldsymbol{n}}\delta_S+\overline{\nabla\cdot\mathbf{D}}+\boldsymbol{n}\cdot[\![\mathbf{D}]\!]\,\delta_S=0, \quad (6)$$

$$(\nabla_\parallel\cdot\mathbf{B}_0)\delta_S+\boldsymbol{n}\cdot\mathbf{B}_0\partial_{\boldsymbol{n}}\delta_S+\overline{\nabla\cdot\mathbf{B}}+\boldsymbol{n}\cdot[\![\mathbf{B}]\!]\,\delta_S=0. \quad (7)$$

Without loss of generality, we can now consider that the interface is surrounded by air (this situation occurs for example in the case of nanoholes arrays in slab waveguides [17]) and use the same decomposition of the susceptibilities as the one for the fields in eq. (3), that is $\overline{\overline{\chi}}_\iota(\boldsymbol{x})=\overline{\overline{\chi}}_{\iota,0}(x,y)\delta_S(\boldsymbol{x})$ for $\iota$ equal to either $ee$ or $mm$. The $\overline{\overline{\chi}}_{\iota,0}$ terms are refereed to as the surfacic susceptibility tensors (and are given in meter). Putting this definition into the constituve relations of eq. (2), one find that the first order fields are linked to the mean value of the regular fields across the interface via the surfacic susceptibilities (see appendix C where the full details of the proof are given). Finally, separating the regular and singular terms in eqs. (4)-(7) we ends up with the following C-GSTCs:

$$\boldsymbol{n}\times[\![\mathbf{E}]\!]=-i\omega\mu_0\left(\overline{\overline{\chi}}_{mm,0}\{\mathbf{H}\}\right)_\parallel+\nabla_\parallel\times\left(\overline{\overline{\chi}}_{ee,0}\{\mathbf{E}\}\right)_\perp, \quad (8)$$

$$\boldsymbol{n}\times[\![\mathbf{H}]\!]=i\omega\varepsilon_0\left(\overline{\overline{\chi}}_{ee,0}\{\mathbf{E}\}\right)_\parallel+\nabla_\parallel\times\left(\overline{\overline{\chi}}_{mm,0}\{\mathbf{H}\}\right)_\perp, \quad (9)$$

$$\boldsymbol{n}\cdot[\![\mathbf{D}]\!]=-\varepsilon_0\nabla_\parallel\cdot\left(\overline{\overline{\chi}}_{ee,0}\{\mathbf{E}\}\right)_\parallel, \quad (10)$$

$$\boldsymbol{n}\cdot[\![\mathbf{B}]\!]=-\mu_0\nabla_\parallel\cdot\left(\overline{\overline{\chi}}_{mm,0}\{\mathbf{H}\}\right)_\parallel. \quad (11)$$

## III. SUSCEPTIBILITY SYNTHESIS

GSTCs provide a way to synthesize the optical response of a shaped metasurface to transform any given incident field into user-defined outgoing transmitted and reflected fields (denoted by $\mathbf{E}_+^0$ and $\mathbf{E}_-^0$ respectively) [18–20]. The results of our synthesis are therefore the coefficient values of the C-GSTCs electric and magnetic surfacic susceptibility tensors $\overline{\overline{\chi}}_{\iota,0}$ as a function of the position along arbitrarily shaped surface. Solutions are obtained by solving the inverse problem in eqs. (8)-(9). Note that no physical assumption has been made so far to restrict the susceptibilities tensors values, leaving us with 12 complex unknown coefficients (due to the symmetry of the susceptibility tensors). Thus, if we consider setting only one incident and one outgoing fields, the solution of the inversion problem is underdetermined. Eqs. (8)-(9) only provide 4 equations in the interface local system of coordinates), indicating that multiple combination of coefficients could satisfy the equations. To obtain a well-posed inversion problem, the most traditional method consists in relying on physical conditions, including for example symmetries and reciprocity such that the C-GSTCs share the same number of equations and unknown susceptibility coefficients. In the following, we consider tensors such that the tangential curl terms in (8)

and (9) vanish. This is a common assumption made with planar GSTC where this term is usually set to zero by taking $\chi_{\iota,0}^{\boldsymbol{\alpha}z} = \chi_{\iota,0}^{z\boldsymbol{\alpha}} = 0$ for $\boldsymbol{\alpha} = \boldsymbol{x}, \boldsymbol{y}, \boldsymbol{z}$ when $\boldsymbol{n} = \boldsymbol{z}$. For nonplanar interface a similar assumption is made using the local orthonormal curvilinear basis $(\boldsymbol{\tau}^1, \boldsymbol{\tau}^2, \boldsymbol{n})$ with tangential vectors $\boldsymbol{\tau}^1$ and $\boldsymbol{\tau}^2$. Given the decomposition of any field $\mathbf{A}$ on $S$ by $\mathbf{A} = (\mathbf{A}\cdot\boldsymbol{\tau}^1)\boldsymbol{\tau}^1 + (\mathbf{A}\cdot\boldsymbol{\tau}^2)\boldsymbol{\tau}^2 + (\mathbf{A}\cdot\boldsymbol{n})\boldsymbol{n}$, the assumption of vanishing tangential curl terms in (8) imposes that the matrices $\overline{\overline{\chi}}_{\iota,0}$ satisfies:

$$\left(\overline{\overline{\chi}}_{\iota,0}\mathbf{A}\right)_{\perp} = \left[\left(\overline{\overline{\chi}}_{\iota,0}\mathbf{A}\right)\cdot\boldsymbol{n}\right]\boldsymbol{n} = \mathbf{0}. \tag{12}$$

Introducing now the general decomposition of the susceptibility tensors in any basis $\mathcal{B}$:

$$\overline{\overline{\chi}}_{\iota,0} = \sum_{\boldsymbol{\alpha},\boldsymbol{\beta}\in\mathcal{B}} \chi_{\iota}^{\boldsymbol{\alpha}\boldsymbol{\beta}}\boldsymbol{\alpha}\otimes\boldsymbol{\beta} \Rightarrow \overline{\overline{\chi}}_{\iota,0}\mathbf{A} = \sum_{\boldsymbol{\alpha},\boldsymbol{\beta}\in\mathcal{B}} \chi_{\iota}^{\boldsymbol{\alpha}\boldsymbol{\beta}}\left(\mathbf{A}\cdot\boldsymbol{\alpha}\right)\boldsymbol{\beta}$$

valid in both Cartesian or curvilinear coordinates considering either $\mathcal{B} = \{\boldsymbol{x}, \boldsymbol{y}, \boldsymbol{z}\}$ or $\mathcal{B} = \{\boldsymbol{\tau}^1, \boldsymbol{\tau}^2, \boldsymbol{n}\}$, eq. (12) leads to $\chi_{\iota,0}^{\boldsymbol{\alpha}\boldsymbol{n}} = 0$ for $\boldsymbol{\alpha} = \boldsymbol{\tau}^1, \boldsymbol{\tau}^2, \boldsymbol{n}$. With this choice of susceptibility tensors, we drastically simplify the first two C-GSTCs into their compact forms:

$$\boldsymbol{n}\times[\![\mathbf{E}]\!] = -i\omega\mu_0\overline{\overline{\chi}}_{mm,0}\left\{\mathbf{H}_{\parallel}\right\}, \tag{13}$$

$$\boldsymbol{n}\times[\![\mathbf{H}]\!] = i\omega\varepsilon_0\overline{\overline{\chi}}_{ee,0}\left\{\mathbf{E}_{\parallel}\right\}. \tag{14}$$

Setting the off-diagonal terms $\chi_{\iota,0}^{\boldsymbol{\tau}^1\boldsymbol{\tau}^2}$ and $\chi_{\iota,0}^{\boldsymbol{\tau}^2\boldsymbol{\tau}^1}$ to zero then leaves only 4 unknown coefficients in the curvilinear coordinate system. In Cartesian coordinates the susceptibilities are then found for $\boldsymbol{\alpha},\boldsymbol{\beta} = \boldsymbol{x},\boldsymbol{y},\boldsymbol{z}$ as $\chi_{\iota,0}^{\boldsymbol{\alpha}\boldsymbol{\beta}} = \chi_{\iota,0}^{\boldsymbol{\tau}^1\boldsymbol{\tau}^1}\boldsymbol{\tau}_{\boldsymbol{\alpha}}^1\boldsymbol{\tau}_{\boldsymbol{\beta}}^1 + \chi_{\iota,0}^{\boldsymbol{\tau}^2\boldsymbol{\tau}^2}\boldsymbol{\tau}_{\boldsymbol{\alpha}}^2\boldsymbol{\tau}_{\boldsymbol{\beta}}^2$. Given injected and transmitted electromagnetic fields $\mathbf{E}_{\pm}^0, \mathbf{H}_{\pm}^0$, the inversion of C-GSTCs eqs. (13)-(14) around the interface leads to:

$$\begin{aligned}
\chi_{ee,0}^{\boldsymbol{\tau}^1\boldsymbol{\tau}^1} &= \frac{-1}{i\omega\varepsilon_0}\frac{[\![\mathbf{H}^0\cdot\boldsymbol{\tau}^2]\!]}{\{\mathbf{E}^0\cdot\boldsymbol{\tau}^1\}}, \quad \chi_{ee,0}^{\boldsymbol{\tau}^2\boldsymbol{\tau}^2} = \frac{1}{i\omega\varepsilon_0}\frac{[\![\mathbf{H}^0\cdot\boldsymbol{\tau}^1]\!]}{\{\mathbf{E}^0\cdot\boldsymbol{\tau}^2\}}, \\
\chi_{mm,0}^{\boldsymbol{\tau}^1\boldsymbol{\tau}^1} &= \frac{1}{i\omega\mu_0}\frac{[\![\mathbf{E}^0\cdot\boldsymbol{\tau}^2]\!]}{\{\mathbf{H}^0\cdot\boldsymbol{\tau}^1\}}, \quad \chi_{mm,0}^{\boldsymbol{\tau}^2\boldsymbol{\tau}^2} = \frac{-1}{i\omega\mu_0}\frac{[\![\mathbf{E}^0\cdot\boldsymbol{\tau}^1]\!]}{\{\mathbf{H}^0\cdot\boldsymbol{\tau}^2\}}.
\end{aligned} \tag{15}$$

## IV. FINITE ELEMENT IMPLEMENTATION

To verify the validity of our C-GSTCs derivation we implemented these equations using the FEM and tested the performance of the synthesized interfaces in terms of angular response efficiency. Incidentally, and to the best of our knowledge, only a recent work dealing with FEM modelling of planar GSTCs in two dimensions has been proposed [21]. Here, we provide a full three-dimensional modelling method that applies to both planar and conformal interfaces. This modelling method relies on the FEM and thus on the variational formulation associated with the vectorial form of the wave equation. In general, this formulation is given in the frequency domain as:

$$\sum_{D\in\mathcal{D}}\int_D \frac{1}{\mu}\nabla\times\mathbf{E}\cdot\nabla\times\boldsymbol{\phi} - k^2\varepsilon\mathbf{E}\cdot\boldsymbol{\phi}\,\mathrm{d}\boldsymbol{x} + B_{\partial D} = 0, \tag{16}$$

where $\mathcal{D}$ is the set of domains present in the simulation and $B_{\partial D}$ is a surfacic integral accounting for the boundary conditions on the domains borders $\partial D$ and given by:

$$B_{\partial D} = -i\omega\mu_0\int_{\partial\mathcal{D}}\boldsymbol{n}\times\mathbf{H}\cdot\boldsymbol{\phi}\,\mathrm{d}\boldsymbol{s}.$$

At the interface $\partial\mathcal{D}_1\cap\partial\mathcal{D}_2$ between two domains, the natural transition conditions gives $\boldsymbol{n}\times[\![\mathbf{H}]\!] = \mathbf{0}$, thus canceling out the surfacic integral. With the C-GSTCs however, the jump of the fields components are not equal to zero and $B_S \neq 0$ (with $S$ the C-GSTCs interface). From eqs. (13)-(14) one find (see appendix E) that $B_S = B_S^{ee,1} + B_S^{ee,2} + B_S^{mm,1} + B_S^{mm,2}$ with:

$$\begin{aligned}
B_S^{ee,\ell} &= -\int_S k_0^2\chi_{ee,0}^{\boldsymbol{\tau}^\ell\boldsymbol{\tau}^\ell}\left\{\mathbf{E}\cdot\boldsymbol{\tau}^\ell\right\}\left\{\boldsymbol{\phi}^*\cdot\boldsymbol{\tau}^\ell\right\}\,\mathrm{d}\boldsymbol{s}, \\
B_S^{mm,\ell} &= \int_S (\chi_{mm,0}^{\boldsymbol{\tau}^\ell\boldsymbol{\tau}^\ell})^{-1}\left[\!\left[\mathbf{E}\cdot\boldsymbol{\tau}^{\bar{\ell}}\right]\!\right]\left[\!\left[\boldsymbol{\phi}^*\cdot\boldsymbol{\tau}^{\bar{\ell}}\right]\!\right]\,\mathrm{d}\boldsymbol{s},
\end{aligned}$$

where $\bar{\ell} = 1$ if $\ell = 2$ and 1 otherwise. One modification of the FEM scheme is also required in order to account for these surfacic integrals. Indeed, the Nédélec elements usually considered in electromagnetic FEM simulations [22, 23] ensure that the natural transition conditions are verified; it considers the same degrees of freedom for the tangential components of the electric field on each side of the interfaces. To account for the C-GSTCs, we instead discretized separately the two domains on each side of $S$ so as to duplicate the number of degree of freedom for the tangential components and thus make it possible to have a non-zero jump of the fields on $S$. The surfacic integrals in $B_S$ together with (16) and additional boundary conditions at the edge of the simulation area to generate an input plane wave and to absorb all outgoing waves (open system) define the whole simulation problem. With respect to existing works dealing with GSTC equations that replace metasurface discontinuous regions with small equivalent volumes [24, section IV. B][25, Section IV], our approach implements directly the real transition conditions inside the variational formulation. Our FEM simulations were performed using `Comsol Multiphysics` in both two and three dimensions [26].

## V. NUMERICAL EXAMPLES

The ability to design arbitrary shaped functional interfaces is of particular interest to study the impact of freeform geometry and compare their performance with respect to conventional flat optical components. We have first realized two simple studies of usual optical components, a lens and a deflector, to illustrate the impact of

interface geometry and how it influence the device optical performance.

### A. Deflector

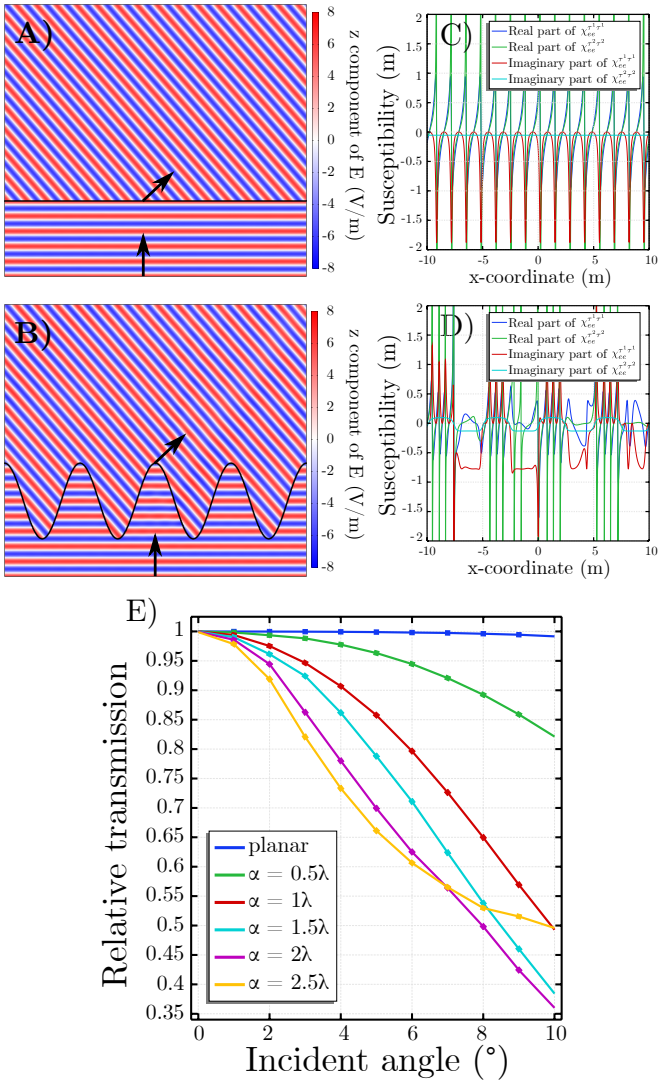


FIG. 2. Planar and sinusoidal light deflectors. A) Flat metasurface deflecting light at an angle $\theta_r^\circ$; B) Similar calculation as in A) but considering a sinusoidal (conformal) interface; C) and D) Associated electric susceptibilities (here $\overline{\overline{\chi}}_{ee} = \overline{\overline{\chi}}_{mm}$) for both planar and conformal metasurfaces; E) Sensitivity of the transmission (normalized by the total output power) into the $\theta_r^\circ$ order of diffraction depending on the amplitude $\alpha$ of the interface's sinusoidal oscillations.

In this first example, we consider a periodically oscillating interface designed using C-GSTCs from which an incident plane wave is refracted at an angle of $\theta_r \simeq 45^\circ$ (the precise value of $\theta_r$ is given by the order of diffraction) with respect to the $\boldsymbol{z}$ axis. We synthesized the susceptibilities using (15) considering $z$-polarized input and output plane waves and the output one given by an order of diffraction with angle $\theta_r$.

The interface geometry is given by $f(x,y) = \alpha\cos(\frac{2\pi}{5\lambda}x)$ for $\alpha$ ranging from 0 to $2.5\lambda$. We implemented the C-GSTCs FEM as mentioned above considering a simulation domain size of $20\lambda \times 20\lambda$ and the results are summarized in Fig. 2.

As we can see in Fig. 2 E) the sinusoidal interface does not perform well when the plane wave is sent with an incident angle different than zero. More precisely, we can see that its performances drastically reduces the deflection efficiency from 100 % to only 50 % for less than 10° incident angle change.

### B. Lens

This example is inspired from pioneering work realized by Ernst Karl Abbe back in 1881 [27]. It states that for any optical system, which would be able to produce on- and off-axis sharp images, the ratio of the sines of the entrance and exit angles $(\alpha_{\text{in}}, \alpha_{\text{out}})$ of optical rays must equal to the magnification $M$ of the optical system with the relationship: $\sin(\alpha_{\text{in}})/\sin(\alpha_{\text{out}}) = |M|$. Ray tracing calculations of light focusing from curved metasurfaces have suggested that Abbe-Sine condition can be realized for spherical interface with radius of curvature equal to the focusing distance of the curved metalens [28] and [29]. C-GSTCs proposed herein have been utilized to calculate the susceptibilities of a focusing half-circle metalens and are used to study the angular response of the Abbe-Sine component. We thus consider the focusing of an incident plane wave from a metalens covering a hemisphere centered at $(0,0,R)$ with radius $R$ while imposing a spherical output wave centered at the focal point $(0,0,f)$. The simulation results are provided in Fig. 3 b)-c) using a domain size of $10\lambda \times 30\lambda$ with $f = 10\lambda$.

To reach the Abbe-Sine condition with curved interfaces, it is necessary to study the focusing responses of metalens for arbitrary incident angles, while keeping the surface susceptibilities initially calculated for normally incident beam. The comparison of both planar versus curved focusing efficiency are presented in Fig. 3 d)-e), including a quantitative comparison with the evolution of the Full Width at Half Maximum (FWHM) in Fig. 3 f). It indicates that the FWHM of the conformal metasurface is almost invariant with respect to the incident angle while it increases for the planar interface case as a function of the incident angle from 0 to 20°. Conformal metasurface are thus able to improve the focusing profile and the point-spread function to reduce monochromatic abberations. In the appendix VI we also present incident angle characterization of a sinusoidal interfaces that are traditionally used for light deflection in generalized Snell-law experiments. We show that instead their deflection efficiency are extremely sensitive to the incident angles.

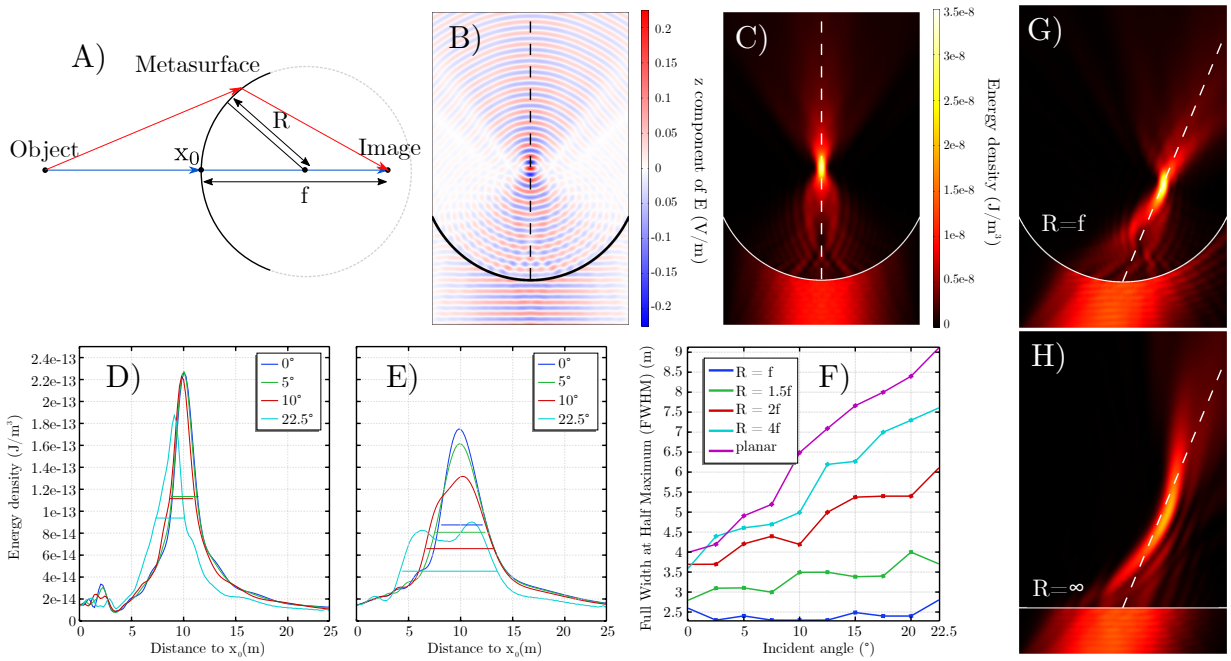


FIG. 3. Planar and conformal metalenses. A) schematic of the Abbe sine numerical experiment realized with curved metalens; B) and C) Calculation of the field transmitted through a synthesized conformal metalens when $R = f$; D) Focusing profile (dashed lines in B)-C) and G)-H) respectively) of the curved metalens when $R = f$; E) Same as D) for the planar metalens; F) Sensitivity of the Full width at half maximum with respect to the incident angle for different radii of curvature of the metasurface. G) and H) Same calculation as in C) but using a plane wave tilted by 22.5° while adjusting the surface curvature to $R = f$ and $R = \text{inf}$ respectively.

### C. Cloaking

In our second example, we realize a new sort of optical illusion, manipulating the optical signature of an actual object, for example a cat-shaped structure, to mimic light scattering of another object, a mouse-shaped structure. Applying a metasurface conformally to the shape on the former object, one can realize an advanced version of cloaking accounting for both the complex shapes and projection of arbitrary field distributions. Our approach suggests wrapping a metasurface conformally to an object, while adjusting the surface susceptibilities, to reflect and/or transmit light as if it was coming from another user-defined object.

The synthesizing of the susceptibilities is realized by computing first the electromagnetic fields scattered by both objects, i.e. cat and mouse-shaped nanostructures in the absence of a metasurface (see Fig. 4 c) and d)), considering an incident plane wave impinging from the bottom left of the simulation domain. We then apply the inversion procedure to adjust the interior fields from the cat geometry to the exterior fields scattered by the mouse shaped structure through the conformal susceptibilities disposed along the cat surface (see Fig. 4 e) ). The calculations are performed considering a background domain with permittivity equal to $\varepsilon_r = 1$ and assuming that the objects are made of homogeneous medium with a permittivity $\varepsilon_r = 2$. The results summarized in Fig. 4 thus indicate that the mouse-scattered fields are reproduced almost perfectly, even from an arbitrary shaped structure, producing the illusion of light scattering from a different object. For practical applications, it is necessary to verify that the scattering illusion is preserved over a relatively large incident angle range. Fig. 4 g) presents the angular cross sections as a function of the incident angles (the outward Poynting vector norm) computed on the edge of the simulation domain (circle boundary). Fig. 4 g) shows that the performance of the illusion system behaves poorly for incident angles slightly different from the designed case. Note that here the susceptibilities have been calculated considering that the field inside the cat-shaped nanostructure remains equal to the field distribution in absence of beam shaping metasurface. Choosing other inner field distribution is also possible. As an example, to study designs with reduced angular sensitivity, we show in Fig. 4 f) that imposing a zero field inside the shaped nanostructure could maintain broader angular scattering.

## VI. CONCLUSION

In conclusion, we have proposed a detailed derivation and full wave implementation of conformal GSTCs. We proposed several numerical examples showing the versatility of the inversion procedure with C-GSTCs. Our pro-

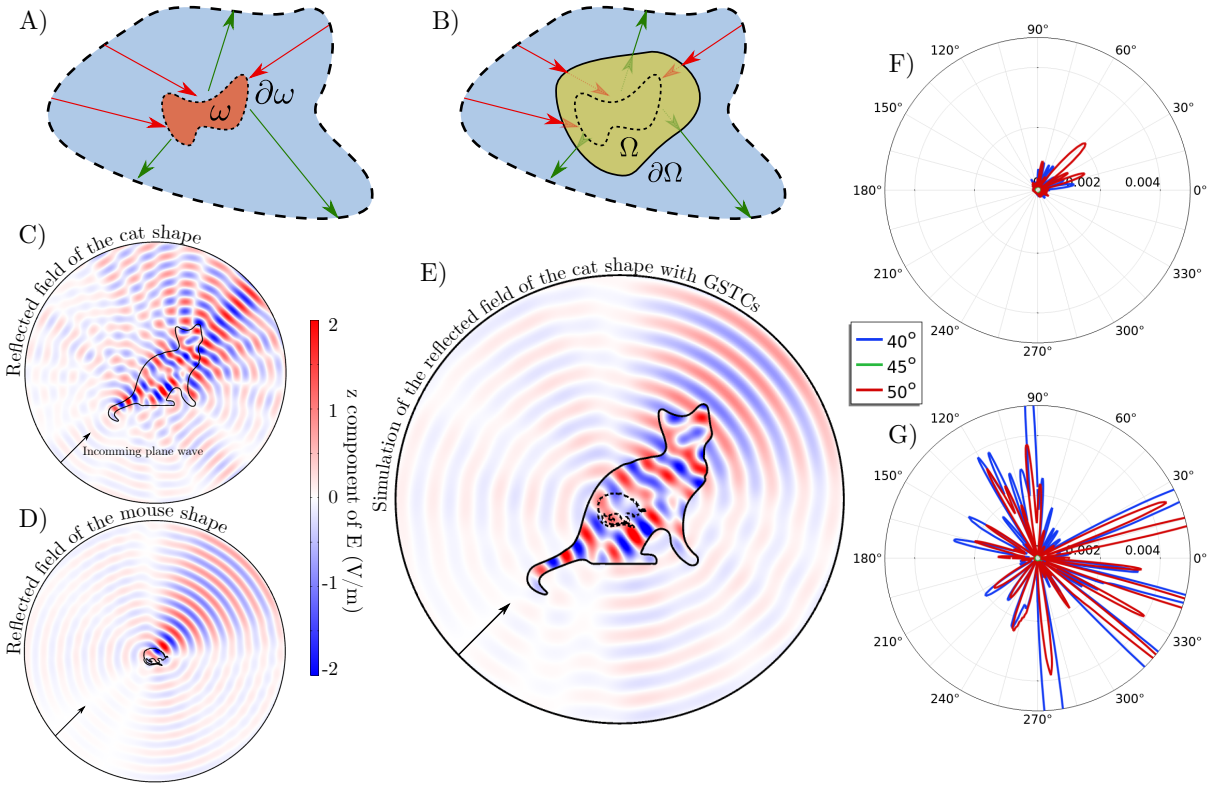


FIG. 4. Conformal metasurface making the cat reflections look like the ones coming from a virtual mouse. A) and B) Schematic representation of the system: a shape $\Omega$ with an optical index equal to 2 is coated with a conformal metasurface on its borders $\partial\Omega$ with susceptibilities synthesized in such a way that the reflections produced by this shape are equal to the one from a non-modified shape $\omega$ with the same optical index; C) and D) Simulation of the reflected field for $\Omega$ (resp. $\omega$) representing a cat (resp. a mouse); E) Simulation of the C-GSTC coated $\Omega$ shape ($\omega$ given for comparison with dashed lines); G) Absolute difference of the outgoing Poynting vectors normal component on the exterior circle between the field reflected by the $\omega$ shape and the C-GSTC coated $\Omega$ one; F) Same as G) but imposing a zero electric field inside the $\Omega$ shape during the susceptibility synthesization step.

posed modeling technique may be of interest to scientists and engineers searching for innovative solutions to adjust the optical response of freeform optical components. However, it is important to keep in mind that even if the presented numerical results may seem promising for future applications of conformal metasurfaces, the susceptibilities obtained through the inversion procedure are not directly linked to physical materials or structures. To alleviate this issue one could for instance consider using susceptibilities coming from the homogenization theory such as in [30, 31]. Other synthesis method could also be considered (and adapted to conformal geometries) such as the one producing physically relevant real-valued susceptibilities in [32].

## ACKNOWLEDGMENTS

The authors acknowledge support from French defence procurement agency under the ANR ASTRID Maturation program, grant agreement number ANR-18-ASMA-0006-01.

## Appendix A: Vectorial identities on surfaces

In all the appendices we consider a surface $S$ embedded in $\mathbb{R}^3$. In terms of notation, we used $[\![\mathbf{A}]\!]$ the jump of the fields $\mathbf{A}$ at the interface and $\boldsymbol{n}$ the associated surface normal vector pointing from the bottom to top domain. The jump $[\![\cdot]\!]$ and mean $\{\cdot\}$ operators are defined for any field $\mathbf{A}$ on $S$ as:

$$[\![\mathbf{A}]\!] = \mathbf{A}^+ - \mathbf{A}^-$$
$$\{\mathbf{A}\} = \frac{\mathbf{A}^+ + \mathbf{A}^-}{2}$$

with $\mathbf{A}^+$ (resp. $\mathbf{A}^-$) the value of $\mathbf{A}$ above (resp. below) the surface $S$.

All the following definitions and properties presented here are fairly classical but we have decided to include them here in order to guide the reader who wants to implement numerically the C-GSTCs.

### 1. Definitions

Let us assume that the surface $S$ is given as the 0 level set of a function $F(x,y,z) = z - f(x,y)$ and that it cut the whole $\mathbb{R}^3$ space into two parts $\mathcal{D}^+ \cup \mathcal{D}^- = \mathcal{D}$ with $\mathcal{D}^+ = \{\boldsymbol{x}, F(\boldsymbol{x}) > 0\}$. For more general surfaces (such as the one in the cloaking example), other definitions of $F$ must be considered. The normal vector $\boldsymbol{n}$ on $S$ pointing into $\mathcal{D}^+$ is then given by:

$$\boldsymbol{n} = \frac{\nabla F}{|\nabla F|} = \frac{(-\partial_x f, -\partial_y f, 1)}{\sqrt{\partial_x f^2 + \partial_y f^2 + 1}}.$$

In the same way, two tangential vectors $\boldsymbol{\tau}^1$ and $\tilde{\boldsymbol{\tau}}^2$ may be found as:

$$\boldsymbol{\tau}^1 = \frac{(1,0,\partial_x f)}{\sqrt{\partial_x f^2 + 1}} \quad \text{and} \quad \tilde{\boldsymbol{\tau}}^2 = \frac{(0,1,\partial_y f)}{\sqrt{\partial_y f^2 + 1}}, \tag{A1}$$

For more general surfaces one need to consider vectors $\boldsymbol{\tau}$ such that $\nabla F \cdot \boldsymbol{\tau} = 0$. For instance if $\partial_z F \neq 0$, fixing $\boldsymbol{\tau}_x = 1, \boldsymbol{\tau}_y = 0$ or the contrary, one find that he need to have $\boldsymbol{\tau}_z = -\partial_x F / \partial_z F$ which leads to eq. (A1). In practice we will consider vectors $(\boldsymbol{\tau}^1, \boldsymbol{\tau}^2, \boldsymbol{n})$ such that it corresponds to an orthonormal basis with:

$$\boldsymbol{n} = \frac{\nabla F}{|\nabla F|}, \quad \boldsymbol{\tau}^1 = \frac{(1,0,\partial_x f)}{\sqrt{\partial_x f^2 + 1}} \quad \text{and} \quad \boldsymbol{\tau}^2 = \boldsymbol{n} \times \boldsymbol{\tau}^1.$$

With this definition we also have $\boldsymbol{\tau}^1 = \boldsymbol{\tau}^2 \times \boldsymbol{n}$. Note also that such a bundle of tangent vectors forming an orthonormal basis is not unique. We define the tangential and normal components of any vector field $\mathbf{A}$ as:

$$\mathbf{A}_\parallel = \boldsymbol{n} \times \mathbf{A} \times \boldsymbol{n} \quad \text{and} \quad \mathbf{A}_\perp = (\mathbf{A} \cdot \boldsymbol{n})\boldsymbol{n} \tag{A2}$$

such that $\mathbf{A} = \mathbf{A}_\parallel + \mathbf{A}_\perp$. The same definitions may be used to define the tangential and normal derivatives by assuming that the nabla (gradient) differential operator $\nabla$ is equal to the vector $(\partial_x, \partial_y, \partial_z)$. This may eventually be written as:

$$\nabla_\parallel = (\mathrm{Id} - \boldsymbol{n} \otimes \boldsymbol{n})\nabla \quad \text{and} \quad \nabla_\perp = (\boldsymbol{n} \otimes \boldsymbol{n})\nabla.$$

For a more precise mathematical definition the reader is referred to [33, Section 5.4].

### 2. Integration by parts

Most of the results from this subsection regarding tangential operators formulas may be found in [23, section 3.4].

#### a. *Integrals involving the curl operator*

First, let us recall the integration by parts formula for the curl on any $\Omega \subset \mathbb{R}^3$ with contour $\partial\Omega$:

$$\int_\Omega \mathbf{A} \cdot \nabla \times \mathbf{B} \mathrm{d}\boldsymbol{x} = \int_\Omega \nabla \times \mathbf{A} \cdot \mathbf{B} \mathrm{d}\boldsymbol{x} + \int_{\partial\Omega} \mathbf{A} \times \boldsymbol{n} \cdot \mathbf{B} \mathrm{d}\boldsymbol{s}. \tag{A3}$$

A similar formula may be obtained for the tangential curl:

$$\int_{\partial\Omega} \nabla_\parallel \times \mathbf{A}_\parallel \cdot \mathbf{B}_\perp \, \mathrm{d}\boldsymbol{s} = \int_{\partial\Omega} \mathbf{A}_\parallel \cdot \nabla_\parallel \times \mathbf{B}_\perp \, \mathrm{d}\boldsymbol{s} + \text{b.t.} \tag{A4}$$

where b.t. corresponds to boundary terms which will be ignored afterward since they are equal to zero for vanishing fields on the edges of $\partial\Omega$ or if $\partial\Omega$ is a closed contour. We will also use the following equality for the curl on a surface:

$$\int_{\partial\Omega} \mathbf{A} \cdot \nabla \times \mathbf{B} \, \mathrm{d}\boldsymbol{s} = \int_{\partial\Omega} \big(\nabla_\parallel \times \mathbf{A}\big) \cdot \mathbf{B} + \underbrace{\mathbf{A}_\parallel \cdot \nabla_\perp \times \mathbf{B}_\parallel}_{(\mathbf{A}_\parallel \times \boldsymbol{n}) \cdot \partial_{\boldsymbol{n}} \mathbf{B}_\parallel} \mathrm{d}\boldsymbol{s} \tag{A5}$$

where $\partial_{\boldsymbol{n}} \mathbf{B}_\parallel = \partial_{\boldsymbol{n}}(\mathbf{B} \cdot \boldsymbol{\tau}_1)\boldsymbol{\tau}_1 + \partial_{\boldsymbol{n}}(\mathbf{B} \cdot \boldsymbol{\tau}_2)\boldsymbol{\tau}_2$. This equation is obtained using the following decomposition and (A4):

$$\begin{aligned}\mathbf{A} \cdot \nabla \times \mathbf{B} = \mathbf{A}_\parallel \cdot \nabla_\perp \times \mathbf{B}_\parallel \\ + \mathbf{A}_\parallel \cdot \nabla_\parallel \times \mathbf{B}_\perp + \mathbf{A}_\perp \cdot \nabla_\parallel \times \mathbf{B}_\parallel.\end{aligned}$$

#### b. *Integrals involving the divergence operator*

Again we remind the reader of the classical integration by parts formula for the divergence on any open subset $\Omega$ of $\mathbb{R}^3$:

$$\int_\Omega (\nabla \cdot \mathbf{A}) \mathrm{B} \, \mathrm{d}\boldsymbol{x} = -\int_\Omega \mathbf{A} \cdot \nabla \mathrm{B} \, \mathrm{d}\boldsymbol{x} + \int_{\partial\Omega} (\boldsymbol{n} \cdot \mathbf{A}) \mathrm{B} \, \mathrm{d}\boldsymbol{s}.$$

Regarding the tangential divergence we will use the relation:

$$\int_{\partial\Omega} \mathbf{A} \cdot \nabla_\parallel \mathrm{B} \, \mathrm{d}\boldsymbol{s} = -\int_{\partial\Omega} (\nabla_\parallel \cdot \mathbf{A}) \mathrm{B} \, \mathrm{d}\boldsymbol{s},$$

which allows to write:

$$\int_{\partial\Omega} \mathbf{A} \cdot \nabla \mathrm{B} \, \mathrm{d}\boldsymbol{s} = -\int_{\partial\Omega} (\nabla_\parallel \cdot \mathbf{A}) \mathrm{B} \, \mathrm{d}\boldsymbol{s} + \int_{\partial\Omega} \underbrace{\mathbf{A} \cdot \nabla_\perp \mathrm{B}}_{(\boldsymbol{n} \cdot \mathbf{A}) \partial_{\boldsymbol{n}} \mathrm{B}} \, \mathrm{d}\boldsymbol{s}$$

using the decomposition:

$$\mathbf{A} \cdot \nabla \mathrm{B} = \mathbf{A} \cdot \nabla_\parallel \mathrm{B} + \mathbf{A} \cdot \nabla_\perp \mathrm{B}.$$

## Appendix B: Dirac distributions on surfaces

### 1. Definition of a Dirac on a surface

The Dirac distribution on the surface $S$ is denoted by $\delta \circ F = \delta_S$ and defined (see for instance [34]) such that for any smooth, and compactly supported function $\phi$ (a.k.a "test function"):

$$\int_{\mathbb{R}^3} \delta_S \phi \, \mathrm{d}\boldsymbol{x} = \int_S \phi \, \mathrm{d}\boldsymbol{s}.$$

With a small abuse of notation we will also use the notation $\delta_S$ for vectorial Dirac surface distributions on $S$.

The derivative of a surface Dirac along the direction $\boldsymbol{\alpha}$ is noted $\partial_{\boldsymbol{\alpha}} \delta_S$ and given for all test functions $\phi$ by:

$$\int_{\mathbb{R}^3} \partial_{\boldsymbol{\alpha}} \delta_S \phi \, \mathrm{d}\boldsymbol{x} = -\int_S \partial_{\boldsymbol{\alpha}} \phi \, \mathrm{d}\boldsymbol{s}. \tag{B1}$$

### 2. Operators on a surface-step functions

We now define a continuous by part step vector-function $\mathbf{A}$ as:

$$\mathbf{A}(x,y,z) = \begin{cases} \mathbf{A}^+(x,y,z) & \text{if } z > f(x,y) \\ \mathbf{A}^-(x,y,z) & \text{if } z < f(x,y) \end{cases}$$

with $\mathbf{A}^+, \mathbf{A}^-$ smooth functions. We also remind the reader that a vectorial function $\mathbf{A}$ is said to have a distributional curl (resp. distributional divergence) if there exist a $\mathbf{g}$ (resp. g) such that for all vectorial test functions $\boldsymbol{\phi}$ (resp. scalar test functions $\phi$):

$$\int_{\mathbb{R}^3} \mathbf{A} \cdot \nabla \times \boldsymbol{\phi} \, \mathrm{d}\boldsymbol{x} = \int_{\mathbb{R}^3} \mathbf{g} \cdot \boldsymbol{\phi} \, \mathrm{d}\boldsymbol{x}, \tag{B2}$$

$$\int_{\mathbb{R}^3} \mathbf{A} \cdot \nabla \phi \, \mathrm{d}\boldsymbol{x} = -\int_{\mathbb{R}^3} g\phi \, \mathrm{d}\boldsymbol{x}. \tag{B3}$$

#### a. Curl

The distributional curl of the step function $\mathbf{A}$ is found using the integration by parts formula of (A3):

$$\begin{aligned}
(\mathrm{B2}) &= \int_{\mathcal{D}^+} \mathbf{A}^+ \cdot \nabla \times \boldsymbol{\phi} \, \mathrm{d}\boldsymbol{x} + \int_{\mathcal{D}^-} \mathbf{A}^- \cdot \nabla \times \boldsymbol{\phi} \, \mathrm{d}\boldsymbol{x} \\
&= \int_{\partial\mathcal{D}^+} \mathbf{A}^+ \times \boldsymbol{n}_{\mathcal{D}^+} \cdot \boldsymbol{\phi} \, \mathrm{d}\boldsymbol{x} + \int_{\partial\mathcal{D}^-} \mathbf{A}^- \times \boldsymbol{n}_{\mathcal{D}^-} \cdot \boldsymbol{\phi} \, \mathrm{d}\boldsymbol{x} \\
&\quad + \int_{\mathcal{D}^+} \nabla \times \mathbf{A}^+ \cdot \boldsymbol{\phi} \, \mathrm{d}\boldsymbol{x} + \int_{\mathcal{D}^-} \nabla \times \mathbf{A}^- \cdot \boldsymbol{\phi} \, \mathrm{d}\boldsymbol{x} \\
&= \int_S [\![\mathbf{A}]\!] \times \boldsymbol{n} \cdot \boldsymbol{\phi} \, \mathrm{d}\boldsymbol{x} + \int_{\mathbb{R}^3} \nabla \times \mathbf{A} \cdot \boldsymbol{\phi} \, \mathrm{d}\boldsymbol{x}
\end{aligned}$$

where we have used the fact that $\boldsymbol{\phi} \to 0$ at infinity. From the definition of the surface Dirac function we thus have:

$$(\mathrm{B2}) = \int_{\mathbb{R}^3} \delta_S \, [\![\mathbf{A}]\!] \times \boldsymbol{n} \cdot \boldsymbol{\phi} + \nabla \times \mathbf{A} \cdot \boldsymbol{\phi} \, \mathrm{d}\boldsymbol{x}$$

We thus find that the distributional curl of $\mathbf{A}$ is $\nabla \times \mathbf{A} + \delta_S \, [\![\mathbf{A}]\!] \times \boldsymbol{n}$.

#### b. Divergence

Here we have to consider the following integral:

$$\begin{aligned}
(\mathrm{B3}) &= \int_{\mathcal{D}^+} \mathbf{A}^+ \cdot \nabla \phi \, \mathrm{d}\boldsymbol{x} + \int_{\mathcal{D}^-} \mathbf{A}^- \cdot \nabla \phi \, \mathrm{d}\boldsymbol{x} \\
&= \int_{\partial\mathcal{D}^+} \mathbf{A}^+ \cdot \boldsymbol{n}_{\mathcal{D}^+} \phi \, \mathrm{d}\boldsymbol{x} + \int_{\partial\mathcal{D}^-} \mathbf{A}^- \cdot \boldsymbol{n}_{\mathcal{D}^-} \phi \, \mathrm{d}\boldsymbol{x} \\
&\quad - \int_{\mathcal{D}^+} \nabla \cdot \mathbf{A}^+ \phi \, \mathrm{d}\boldsymbol{x} - \int_{\mathcal{D}^-} \nabla \cdot \mathbf{A}^- \phi \, \mathrm{d}\boldsymbol{x} \\
&= \int_{\mathbb{R}^3} \delta_S \, [\![\mathbf{A}]\!] \cdot \boldsymbol{n} \phi - \nabla \cdot \mathbf{A} \phi \, \mathrm{d}\boldsymbol{x},
\end{aligned}$$

which gives the distributional divergence of $\mathbf{A}$ as $\nabla \cdot \mathbf{A} + \delta_S \, [\![\mathbf{A}]\!] \cdot \boldsymbol{n}$.

### 3. Operators for the product between a function and a surface Dirac

#### a. Curl

With the same method as in appendix B 2 using the integration by parts formula of equation (A5) we find that (for $\mathbf{A}$ defined on $S$):

$$\begin{aligned}
\int_{\mathbb{R}^3} (\mathbf{A}\delta_S) \cdot \nabla \times \boldsymbol{\phi} \, \mathrm{d}\boldsymbol{x} &= \int_S \mathbf{A} \cdot \nabla \times \boldsymbol{\phi} \, \mathrm{d}\boldsymbol{s} \\
&= \int_S (\nabla_\parallel \times \mathbf{A}) \cdot \boldsymbol{\phi} \, \mathrm{d}\boldsymbol{s} + \int_S (\mathbf{A}_\parallel \times \boldsymbol{n}) \cdot \partial_{\boldsymbol{n}} \boldsymbol{\phi}_\parallel \, \mathrm{d}\boldsymbol{s}
\end{aligned}$$

Using the definition of the Dirac derivative in (B2) we then find that the curl of $\mathbf{A}\delta_S$ is given as $(\nabla_\parallel \times \mathbf{A})\delta_S + \boldsymbol{n} \times \mathbf{A}_\parallel \partial_{\boldsymbol{n}} \delta_S$.

#### b. Divergence

In the same way we have:

$$\begin{aligned}
\int_{\mathbb{R}^3} (\mathbf{A}\delta_S) \cdot \nabla \phi \, \mathrm{d}\boldsymbol{x} &= \int_S \mathbf{A} \cdot \nabla \phi \, \mathrm{d}\boldsymbol{s} \\
&= -\int_S (\nabla_\parallel \cdot \mathbf{A}) \phi \, \mathrm{d}\boldsymbol{s} + \int_S \boldsymbol{n} \cdot \mathbf{A} (\partial_{\boldsymbol{n}} \phi) \, \mathrm{d}\boldsymbol{s}
\end{aligned}$$

The divergence of $\mathbf{A}\delta_S$ is thus given as $(\nabla_\parallel \cdot \mathbf{A})\delta_S + \boldsymbol{n} \cdot \mathbf{A} \partial_{\boldsymbol{n}} \delta_S$.

### c. Identities

We summarize in this subsection the identities discussed above.

For any "singular" field $\mathbf{A}_0$ defined on the surface $S$:

$$\nabla \times (\mathbf{A}_0 \delta_S) = (\nabla_\parallel \times \mathbf{A}_0)\delta_S + \boldsymbol{n} \times \mathbf{A}_0 \partial_{\boldsymbol{n}} \delta_S,$$
$$\nabla \cdot (\mathbf{A}_0 \delta_S) = (\nabla_\parallel \cdot \mathbf{A}_0)\delta_S + \boldsymbol{n} \cdot \mathbf{A}_0 \partial_{\boldsymbol{n}} \delta_S.$$

For any "regular" field $\overline{\mathbf{A}}$ defined in the whole space:

$$\nabla \times \overline{\mathbf{A}} = \overline{\nabla \times \mathbf{A}} + \boldsymbol{n} \times [\![\mathbf{A}]\!]\, \delta_S,$$
$$\nabla \cdot \overline{\mathbf{A}} = \overline{\nabla \cdot \mathbf{A}} + \boldsymbol{n} \cdot [\![\mathbf{A}]\!]\, \delta_S.$$

## Appendix C: Full derivation of C-GSTCs

Note that readers interested in the derivation for the planar case could refer to [20, Appendix A] [14] and [35].

We recall that we consider the following Maxwell equations:

$$\begin{array}{rclcrcl} \nabla \times \mathbf{E} &=& -i\omega \mathbf{B}, & & \nabla \times \mathbf{H} &=& i\omega \mathbf{D}, \\ \nabla \cdot \mathbf{D} &=& 0, & & \nabla \cdot \mathbf{B} &=& 0, \end{array} \tag{C1}$$

with the constitutive relations

$$\mathbf{D} = \varepsilon_0(\overline{\overline{\chi}}_{ee} + 1)\mathbf{E}, \quad \mathbf{B} = \mu_0(\overline{\overline{\chi}}_{mm} + 1)\mathbf{H}. \tag{C2}$$

Note however that the general case with $\mathbf{D} = \varepsilon_0(\mathbf{E} + \mathbf{P})$ and $\mathbf{B} = \mu_0 \mathbf{H} + \mathbf{M}$ may be considered (for instance if one is interested in bi-anisotropic materials where $\mathbf{D} = \varepsilon \mathbf{E} + \xi \mathbf{H}$, $\mathbf{B} = \mu \mathbf{H} + \zeta \mathbf{E}$) in our analysis but additional assumptions on the polarization and magnetization fields will be required in order link their first order singular values with the regular fields. We consider the following decomposition of the fields:

$$\mathbf{A}(\boldsymbol{x}) = \overline{\mathbf{A}}(\boldsymbol{x}) + \sum_{n=0}^{\infty} \mathbf{A}_n(x,y)\delta_S^{(n)}(\boldsymbol{x}). \tag{C3}$$

A similar decomposition is also assumed for the susceptibilities. To further simplify the analysis, we consider, without loss of generality, that the metasurface is embedded in air. The regular part of the susceptibilities thus vanishes and gives for $\iota = ee, mm$:

$$\overline{\overline{\chi}}_\iota(\boldsymbol{x}) = \sum_{n=0}^{\infty} \overline{\overline{\chi}}_{\iota,n}(x,y)\delta_S^{(n)}(\boldsymbol{x}), \tag{C4}$$

where $\overline{\overline{\chi}}_{\iota,n}$ is referred to as the $n$-th surfacic susceptibility tensor. These singular decompositions may be seen as a limit case of the classical Taylor expansion for functions which became discontinuous as the thickness of the interface tends to zero. Indeed, the $n$-th derivative of a discontinuous function is given by $\delta^{(n-1)}$ and the surfacic susceptibilities are then none other than the coefficients present in the Taylor expansion. This remark shows that $\overline{\overline{\chi}}_{\iota,n}$ is proportional to $\ell^{n+1}$ (where $\ell$ is the thickness of the interface) and thus that it is expressed in meter to the power $n$+1. It also suggests that by considering sufficiently thin interfaces we should have $\mathbf{A}_n = \overline{\overline{\chi}}_{ee,n} = \overline{\overline{\chi}}_{mm,n} = 0$ for $n > 0$ since the first order effects in the expansion are dominant.

Injecting these decompositions into Maxwell equations we find that:

$$\nabla \times \left(\mathbf{E}_0 \delta_S + \overline{\mathbf{E}}\right) = -i\omega \left(\mathbf{B}_0 \delta_S + \overline{\mathbf{B}}\right), \tag{C5}$$
$$\nabla \times \left(\mathbf{H}_0 \delta_S + \overline{\mathbf{H}}\right) = i\omega \left(\mathbf{D}_0 \delta_S + \overline{\mathbf{D}}\right), \tag{C6}$$
$$\nabla \cdot \left(\mathbf{D}_0 \delta_S + \overline{\mathbf{D}}\right) = 0, \tag{C7}$$
$$\nabla \cdot \left(\mathbf{B}_0 \delta_S + \overline{\mathbf{B}}\right) = 0. \tag{C8}$$

Now considering the identities of section B 3 c these equations are modified into:

$$(\nabla_\parallel \times \mathbf{E}_0)\delta_S + \boldsymbol{n} \times \mathbf{E}_0 \partial_{\boldsymbol{n}} \delta_S + \overline{\nabla \times \mathbf{E}} + \boldsymbol{n} \times [\![\mathbf{E}]\!]\, \delta_S = -i\omega \left(\mathbf{B}_0 \delta_S + \overline{\mathbf{B}}\right),$$
$$(\nabla_\parallel \times \mathbf{H}_0)\delta_S + \boldsymbol{n} \times \mathbf{H}_0 \partial_{\boldsymbol{n}} \delta_S + \overline{\nabla \times \mathbf{H}} + \boldsymbol{n} \times [\![\mathbf{H}]\!]\, \delta_S = i\omega \left(\mathbf{D}_0 \delta_S + \overline{\mathbf{D}}\right),$$
$$(\nabla_\parallel \cdot \mathbf{D}_0)\delta_S + \boldsymbol{n} \cdot \mathbf{D}_0 \partial_{\boldsymbol{n}} \delta_S + \overline{\nabla \cdot \mathbf{D}} + \boldsymbol{n} \cdot [\![\mathbf{D}]\!]\, \delta_S = 0,$$
$$(\nabla_\parallel \cdot \mathbf{B}_0)\delta_S + \boldsymbol{n} \cdot \mathbf{B}_0 \partial_{\boldsymbol{n}} \delta_S + \overline{\nabla \cdot \mathbf{B}} + \boldsymbol{n} \cdot [\![\mathbf{B}]\!]\, \delta_S = 0.$$

Splitting these previous equations between similar singularities, we obtain for the regular part:

$$\overline{\nabla \times \mathbf{E}} = -i\omega \overline{\mathbf{B}}, \ \overline{\nabla \times \mathbf{H}} = i\omega \overline{\mathbf{D}}, \ \overline{\nabla \cdot \mathbf{D}} = 0, \ \overline{\nabla \cdot \mathbf{B}} = 0,$$

from which we infer that the regular part of the fields are solutions to the classical Maxwell equations. The simply singular parts (sorting terms in front of $\delta_S$) implies that:

$$\begin{array}{rcl} \nabla_\parallel \times \mathbf{E}_0 + \boldsymbol{n} \times [\![\mathbf{E}]\!] &=& -i\omega \mathbf{B}_0, \\ \nabla_\parallel \times \mathbf{H}_0 + \boldsymbol{n} \times [\![\mathbf{H}]\!] &=& i\omega \mathbf{D}_0, \\ \nabla_\parallel \cdot \mathbf{D}_0 + \boldsymbol{n} \cdot [\![\mathbf{D}]\!] &=& 0, \\ \nabla_\parallel \cdot \mathbf{B}_0 + \boldsymbol{n} \cdot [\![\mathbf{B}]\!] &=& 0. \end{array} \tag{C9}$$

Note here that once the first order singularities $\mathbf{A}_0$ are known, these previous equations gives the transition conditions verified by the fields. The "second order" singular parts (terms in front of $\partial_{\boldsymbol{n}} \delta_S$) gives:

$$\boldsymbol{n} \times \mathbf{E}_0 = \mathbf{0}, \ \boldsymbol{n} \times \mathbf{H}_0 = \mathbf{0}, \ \boldsymbol{n} \cdot \mathbf{D}_0 = 0, \ \boldsymbol{n} \cdot \mathbf{B}_0 = 0, \tag{C10}$$

which may be interpreted as the fact the first order singularities verifies the natural transition conditions.

The same manipulation may be done in the constitutive relations of (C2) using the decomposition (C4) for

any $\boldsymbol{x}$ with $z \neq f(x,y)$:

$$\overline{\mathbf{D}} + \mathbf{D}_0\delta_S = \varepsilon_0(\overline{\overline{\chi}}_{ee,0}\delta_S + 1)(\overline{\mathbf{E}} + \mathbf{E}_0\delta_S), \tag{C11}$$
$$\overline{\mathbf{B}} + \mathbf{B}_0\delta_S = \mu_0(\overline{\overline{\chi}}_{mm,0}\delta_S + 1)(\overline{\mathbf{H}} + \mathbf{H}_0\delta_S). \tag{C12}$$

This gives for the simply singular terms:

$$\mathbf{D}_0 = \varepsilon_0\left(\overline{\overline{\chi}}_{ee,0}\overline{\mathbf{E}} + \mathbf{E}_0\right),\ \mathbf{B}_0 = \mu_0\left(\overline{\overline{\chi}}_{mm,0}\overline{\mathbf{H}} + \mathbf{H}_0\right). \tag{C13}$$

Note however that equations (C11)-(C12) are not well-defined since they involve the product of two Dirac distributions. By passing to the limit on the interface we can write (C13) for any $\boldsymbol{x}$ such that $z = f(x,y)$ as (since the regular part may be chosen as either the top or bottom values):

$$\mathbf{D}_0 = \varepsilon_0\left(\overline{\overline{\chi}}_{ee,0}\{\mathbf{E}\} + \mathbf{E}_0\right),\ \mathbf{B}_0 = \mu_0\left(\overline{\overline{\chi}}_{mm,0}\{\mathbf{H}\} + \mathbf{H}_0\right). \tag{C14}$$

These constitutive relations may also be seen as $\mathbf{D}_0 = \varepsilon_0\mathbf{E}_0 + \mathbf{P}_0$ and $\mathbf{B}_0 = \mu_0\mathbf{H}_0 + \mathbf{M}_0$ where the polarization $\mathbf{P}_0$ and magnetization $\mathbf{M}_0$ are given by $\mathbf{P}_0 = \varepsilon_0\overline{\overline{\chi}}_{ee,0}\{\mathbf{E}\}$ and $\mathbf{M}_0 = \mu_0\overline{\overline{\chi}}_{mm,0}\{\mathbf{H}\}$ (note that in [35, Section 4.3.1] the author directly assume that the polarization and magnetization are given by such relations while we tried here to justify such expressions through equations (C11)-(C12), although a proper justification of these relations is only found through the homogenization theory as it was done in [30, 31]). Now, by taking the scalar and cross product of the constitutive relations (C14) with the normal vector $\boldsymbol{n}$ and using eq. (C10) we find that:

$$\begin{aligned}
\boldsymbol{n}\cdot\mathbf{E}_0 &= -\boldsymbol{n}\cdot\overline{\overline{\chi}}_{ee}\{\mathbf{E}\}, \quad \boldsymbol{n}\times\mathbf{D}_0 = \varepsilon_0\boldsymbol{n}\times\left(\overline{\overline{\chi}}_{ee}\{\mathbf{E}\}\right),\\
\boldsymbol{n}\cdot\mathbf{H}_0 &= -\boldsymbol{n}\cdot\overline{\overline{\chi}}_{mm}\{\mathbf{H}\}, \quad \boldsymbol{n}\times\mathbf{B}_0 = \mu_0\boldsymbol{n}\times\left(\overline{\overline{\chi}}_{mm}\{\mathbf{H}\}\right).
\end{aligned}$$

Now using the notation of (A2) ($\mathbf{A}_{0,\parallel} = \boldsymbol{n}\times\mathbf{A}_0\times\boldsymbol{n}$, $\mathbf{A}_{0,\perp} = (\mathbf{A}_0\cdot\boldsymbol{n})\boldsymbol{n}$) these last equations may be written as:

$$\begin{aligned}
\mathbf{E}_{0,\perp} &= -\left(\overline{\overline{\chi}}_{ee}\{\mathbf{E}\}\right)_\perp, \quad \mathbf{D}_{0,\parallel} = \varepsilon_0\left(\overline{\overline{\chi}}_{ee}\{\mathbf{E}\}\right)_\parallel\\
\mathbf{H}_{0,\perp} &= -\left(\overline{\overline{\chi}}_{mm}\{\mathbf{H}\}\right)_\perp, \quad \mathbf{B}_{0,\parallel} = \mu_0\left(\overline{\overline{\chi}}_{mm}\{\mathbf{H}\}\right)_\parallel,
\end{aligned}$$

while (C10) gives:

$$\mathbf{E}_{0,\parallel} = 0, \quad \mathbf{H}_{0,\parallel} = 0, \quad \mathbf{D}_{0,\perp} = 0, \quad \mathbf{B}_{0,\perp} = 0,$$

meaning that using the decomposition $\mathbf{A}_0 = \mathbf{A}_{0,\parallel} + \mathbf{A}_{0,\perp}$ we have the following expressions of the first order singularities:

$$\begin{aligned}
\mathbf{E}_0 &= -\left(\overline{\overline{\chi}}_{ee}\{\mathbf{E}\}\right)_\perp, \quad \mathbf{D}_0 = \varepsilon_0\left(\overline{\overline{\chi}}_{ee}\{\mathbf{E}\}\right)_\parallel,\\
\mathbf{H}_0 &= -\left(\overline{\overline{\chi}}_{mm}\{\mathbf{H}\}\right)_\perp, \quad \mathbf{B}_0 = \mu_0\left(\overline{\overline{\chi}}_{mm}\{\mathbf{H}\}\right)_\parallel.
\end{aligned} \tag{C15}$$

Finding the C-GSTCs then amounts to injecting these expressions into the previously found equations (C9):

$$\begin{aligned}
\boldsymbol{n}\times[\![\mathbf{E}]\!] &= -i\omega\mu_0\left(\overline{\overline{\chi}}_{mm,0}\{\mathbf{H}\}\right)_\parallel + \nabla_\parallel\times\left(\overline{\overline{\chi}}_{ee,0}\{\mathbf{E}\}\right)_\perp,\\
\boldsymbol{n}\times[\![\mathbf{H}]\!] &= i\omega\varepsilon_0\left(\overline{\overline{\chi}}_{ee,0}\{\mathbf{E}\}\right)_\parallel + \nabla_\parallel\times\left(\overline{\overline{\chi}}_{mm,0}\{\mathbf{H}\}\right)_\perp,\\
\boldsymbol{n}\cdot[\![\mathbf{D}]\!] &= -\varepsilon_0\nabla_\parallel\cdot\left(\overline{\overline{\chi}}_{ee,0}\{\mathbf{E}\}\right)_\parallel,\\
\boldsymbol{n}\cdot[\![\mathbf{B}]\!] &= -\mu_0\nabla_\parallel\cdot\left(\overline{\overline{\chi}}_{mm,0}\{\mathbf{H}\}\right)_\parallel,
\end{aligned}$$

Note that these equations reduce to the GSTCs reported in [20, Eq. (2a)-(2d)] for a planar interface with $\boldsymbol{n} = \boldsymbol{z}$ and the operators $\nabla_\parallel, (\cdot)_\perp, (\cdot)_\parallel$ defined on the conformal interface (see equation (A2)).

## Appendix D: The two-dimensional case

We propose in this appendix details on the simplification of C-GSTCs in two dimensions. This section may be useful for those who want to implement by themselves these boundary conditions and test them on small and easier cases, or simply to understand our two-dimensional model. Here, we consider two-dimensional materials and sources with an invariance in the $y$ direction, meaning that all the $y$ partial derivatives are equal to zero. This lead to two independents triplets of fields coordinates, namely the Transverse Electric (TE) for $(\mathbf{E}_x, \mathbf{H}_y, \mathbf{E}_z)$ and Transverse Magnetic (TM) for $(\mathbf{H}_x, \mathbf{E}_y, \mathbf{H}_z)$ with $\mathbf{E}_y$ and $\mathbf{H}_y$ solutions to scalar wave equations (with $\nabla = (\partial_x, 0, \partial_z)$):

$$\begin{aligned}
-\nabla\cdot\left(\frac{1}{\mu}\nabla\mathbf{E}_y\right) - k_0^2\varepsilon\mathbf{E}_y = 0,\\
-\nabla\cdot\left(\frac{1}{\varepsilon}\nabla\mathbf{H}_y\right) - k_0^2\mu\mathbf{H}_y = 0,
\end{aligned}$$

complemented by the following relations:

$$\mathbf{E}_x = \frac{-\partial_z\mathbf{H}_y}{i\omega\varepsilon_0},\ \mathbf{E}_z = \frac{\partial_x\mathbf{H}_y}{i\omega\varepsilon_0},\ \mathbf{H}_x = \frac{\partial_z\mathbf{E}_y}{i\omega\mu_0},\ \mathbf{H}_z = \frac{-\partial_x\mathbf{E}_y}{i\omega\mu_0}.$$

For any interface we also have $\boldsymbol{n} = (\boldsymbol{n}_x, 0, \boldsymbol{n}_z)$, $\boldsymbol{\tau}^1 = (\boldsymbol{\tau}_x, 0, \boldsymbol{\tau}_z)$ with $\boldsymbol{\tau}_x = \boldsymbol{n}_z, \boldsymbol{\tau}_z = -\boldsymbol{n}_x$ and $\boldsymbol{\tau}^2 = \boldsymbol{n}\times\boldsymbol{\tau}^1 = (0,1,0)$. The C-GSTCs reduces to the following systems for TM:

$$\begin{aligned}
-[\![\mathbf{E}_y]\!] &= -i\omega\mu_0\chi_{mm}^{\boldsymbol{\tau}^1\boldsymbol{\tau}^1}(\boldsymbol{\tau}_x\{\mathbf{H}_x\} + \boldsymbol{\tau}_z\{\mathbf{H}_z\}),\\
\boldsymbol{n}_z[\![\mathbf{H}_x]\!] - \boldsymbol{n}_x[\![\mathbf{H}_z]\!] &= i\omega\varepsilon_0\chi_{ee}^{\boldsymbol{\tau}^2\boldsymbol{\tau}^2}\{\mathbf{E}_y\},
\end{aligned}$$

where we used the fact that $\boldsymbol{n}_x\boldsymbol{\tau}_z - \boldsymbol{n}_z\boldsymbol{\tau}_x = -1$. Similarly for the TE polarization:

$$\begin{aligned}
\boldsymbol{n}_z[\![\mathbf{E}_x]\!] - \boldsymbol{n}_x[\![\mathbf{E}_z]\!] &= -i\omega\mu_0\chi_{mm}^{\boldsymbol{\tau}^2\boldsymbol{\tau}^2}\{\mathbf{H}_y\},\\
-[\![\mathbf{H}_y]\!] &= i\omega\varepsilon_0\chi_{ee}^{\boldsymbol{\tau}^1\boldsymbol{\tau}^1}(\boldsymbol{\tau}_x\{\mathbf{E}_x\} + \boldsymbol{\tau}_z\{\mathbf{E}_z\}),
\end{aligned}$$

meaning that only $\chi_{ee}^{\boldsymbol{\tau}^1\boldsymbol{\tau}^1}$ and $\chi_{mm}^{\boldsymbol{\tau}^2\boldsymbol{\tau}^2}$ are used for the TE polarization while $\chi_{ee}^{\boldsymbol{\tau}^2\boldsymbol{\tau}^2}$, $\chi_{mm}^{\boldsymbol{\tau}^1\boldsymbol{\tau}^1}$ are used in the TM case.

The susceptibilities are obtained through the inversion procedure as:

$$\chi_{ee}^{\boldsymbol{\tau}^1\boldsymbol{\tau}^1} = \frac{-1}{i\omega\varepsilon_0}\frac{[\![\mathbf{H}_y^0]\!]}{\boldsymbol{\tau}_x\{\mathbf{E}_x^0\}+\boldsymbol{\tau}_z\{\mathbf{E}_z^0\}},$$
$$\chi_{ee}^{\boldsymbol{\tau}^2\boldsymbol{\tau}^2} = \frac{1}{i\omega\varepsilon_0}\frac{\boldsymbol{\tau}_x[\![\mathbf{H}_x^0]\!]+\boldsymbol{\tau}_z[\![\mathbf{H}_z^0]\!]}{\{\mathbf{E}_y^0\}},$$
$$\chi_{mm}^{\boldsymbol{\tau}^1\boldsymbol{\tau}^1} = \frac{1}{i\omega\mu_0}\frac{[\![\mathbf{E}_y^0]\!]}{\boldsymbol{\tau}_x\{\mathbf{H}_x^0\}+\boldsymbol{\tau}_z\{\mathbf{H}_z^0\}},$$
$$\chi_{mm}^{\boldsymbol{\tau}^2\boldsymbol{\tau}^2} = \frac{-1}{i\omega\mu_0}\frac{\boldsymbol{\tau}_x[\![\mathbf{E}_x^0]\!]+\boldsymbol{\tau}_z[\![\mathbf{E}_z^0]\!]}{\{\mathbf{H}_y^0\}}.$$

## Appendix E: Full derivation of the variational formulation

We remind the reader that the variational formulation associated with Maxwell equations in the frequency domain is obtained from the vector wave equation:

$$\nabla\times\nabla\times\mathbf{E} - k^2\varepsilon_r\mathbf{E} = 0.$$

Note that we consider here the case of constant permeability only for simplicity of the following equations but this is not a mandatory assumption. Taking the scalar product of this equation with a test function $\boldsymbol{\phi}$ and integrating on the domain $D$ we find that:

$$\int_D \nabla\times\nabla\times\mathbf{E}\cdot\boldsymbol{\phi} - k^2\varepsilon_r\mathbf{E}\cdot\boldsymbol{\phi}\,\mathrm{d}\boldsymbol{x} = 0.$$

Using the curl integration by part formula of (A3) we then obtain:

$$\int_D \nabla\times\mathbf{E}\cdot\nabla\times\boldsymbol{\phi} - k^2\varepsilon_r\mathbf{E}\cdot\boldsymbol{\phi}\,\mathrm{d}\boldsymbol{x} + B_{\partial D} = 0, \quad \text{(E1)}$$

where

$$B_{\partial D} = \int_{\partial D}\boldsymbol{n}\times\nabla\times\mathbf{E}\cdot\boldsymbol{\phi}\,\mathrm{d}\boldsymbol{s} = -i\omega\mu_0\int_{\partial D}\boldsymbol{n}\times\mathbf{H}\cdot\boldsymbol{\phi}\,\mathrm{d}\boldsymbol{s}.$$

Now if there is two domains $\mathcal{D}^+$ and $\mathcal{D}^-$ sharing a common surface $S$, the sum of the associated variational formulation gives:

$$\sum_{\iota\in\{+,-\}}\int_{D^\iota}\nabla\times\mathbf{E}\cdot\nabla\times\boldsymbol{\phi} - k^2\varepsilon_r\mathbf{E}\cdot\boldsymbol{\phi}\,\mathrm{d}\boldsymbol{x} + B_{\partial D^\iota} = 0,$$

with the common boundary terms given by:

$$\begin{aligned}B_S &= B_{\partial D^+\cap S} + B_{\partial D^-\cap S}\\ &= i\omega\mu_0\int_S [\![\boldsymbol{n}\times\mathbf{H}\cdot\boldsymbol{\phi}]\!]\,\mathrm{d}\boldsymbol{s}\\ &= i\omega\mu_0\int_S \boldsymbol{n}\times[\![\mathbf{H}]\!]\cdot\{\boldsymbol{\phi}\} + \boldsymbol{n}\times\{\mathbf{H}\}\cdot[\![\boldsymbol{\phi}]\!]\,\mathrm{d}\boldsymbol{s}\end{aligned}$$

where $\boldsymbol{n}$ is pointing from $D^-$ to $D^+$. The terms inside this last integral may be written using solely their tangential components using that

$$\boldsymbol{n}\times[\![\mathbf{H}]\!]\cdot\{\boldsymbol{\phi}\} = ([\![\mathbf{H}]\!]\cdot\boldsymbol{\tau}^1)(\{\boldsymbol{\phi}\}\cdot\boldsymbol{\tau}^2) - ([\![\mathbf{H}]\!]\cdot\boldsymbol{\tau}^2)(\{\boldsymbol{\phi}\}\cdot\boldsymbol{\tau}^1),$$
$$\boldsymbol{n}\times\{\mathbf{H}\}\cdot[\![\boldsymbol{\phi}]\!] = (\{\mathbf{H}\}\cdot\boldsymbol{\tau}^1)([\![\boldsymbol{\phi}]\!]\cdot\boldsymbol{\tau}^2) - (\{\mathbf{H}\}\cdot\boldsymbol{\tau}^2)([\![\boldsymbol{\phi}]\!]\cdot\boldsymbol{\tau}^1).$$

Now, thanks to the definition of the susceptibilities, one can see that the C-GSTCs may be expressed as (by taking the dot products with $\boldsymbol{\tau}^1$ and $\boldsymbol{\tau}^2$):

$$\begin{aligned}\boldsymbol{n}\times[\![\mathbf{E}]\!]\cdot\boldsymbol{\tau}^1 &= -i\omega\mu_0\chi_{mm}^{\boldsymbol{\tau}^1\boldsymbol{\tau}^1}\{\mathbf{H}\}\cdot\boldsymbol{\tau}^1,\\ \boldsymbol{n}\times[\![\mathbf{E}]\!]\cdot\boldsymbol{\tau}^2 &= -i\omega\mu_0\chi_{mm}^{\boldsymbol{\tau}^2\boldsymbol{\tau}^2}\{\mathbf{H}\}\cdot\boldsymbol{\tau}^2,\\ \boldsymbol{n}\times[\![\mathbf{H}]\!]\cdot\boldsymbol{\tau}^1 &= i\omega\varepsilon_0\chi_{ee}^{\boldsymbol{\tau}^1\boldsymbol{\tau}^1}\{\mathbf{E}\}\cdot\boldsymbol{\tau}^1,\\ \boldsymbol{n}\times[\![\mathbf{H}]\!]\cdot\boldsymbol{\tau}^2 &= i\omega\varepsilon_0\chi_{ee}^{\boldsymbol{\tau}^2\boldsymbol{\tau}^2}\{\mathbf{E}\}\cdot\boldsymbol{\tau}^2.\end{aligned}$$

Or equivalently:

$$\begin{aligned}\{\mathbf{H}\cdot\boldsymbol{\tau}^1\} &= \frac{1}{i\omega\mu_0}(\chi_{mm}^{\boldsymbol{\tau}^1\boldsymbol{\tau}^1})^{-1}[\![\mathbf{E}\cdot\boldsymbol{\tau}^2]\!],\\ \{\mathbf{H}\cdot\boldsymbol{\tau}^2\} &= \frac{-1}{i\omega\mu_0}(\chi_{mm}^{\boldsymbol{\tau}^2\boldsymbol{\tau}^2})^{-1}[\![\mathbf{E}\cdot\boldsymbol{\tau}^1]\!],\\ [\![\mathbf{H}\cdot\boldsymbol{\tau}^2]\!] &= -i\omega\varepsilon_0\chi_{ee}^{\boldsymbol{\tau}^1\boldsymbol{\tau}^1}\{\mathbf{E}\cdot\boldsymbol{\tau}^1\},\\ [\![\mathbf{H}\cdot\boldsymbol{\tau}^1]\!] &= i\omega\varepsilon_0\chi_{ee}^{\boldsymbol{\tau}^2\boldsymbol{\tau}^2}\{\mathbf{E}\cdot\boldsymbol{\tau}^2\}.\end{aligned}$$

We thus find that the surface integrals may be simplified into $B_S = B_S^{ee,1} + B_S^{ee,2} + B_S^{mm,1} + B_S^{mm,2}$ with:

$$\begin{aligned}B_S^{ee,1} &= -\int_S k_0^2\chi_{ee}^{\boldsymbol{\tau}^1\boldsymbol{\tau}^1}\{\mathbf{E}\cdot\boldsymbol{\tau}^1\}\{\boldsymbol{\phi}^*\cdot\boldsymbol{\tau}^1\}\,\mathrm{d}\boldsymbol{s},\\ B_S^{ee,2} &= -\int_S k_0^2\chi_{ee}^{\boldsymbol{\tau}^2\boldsymbol{\tau}^2}\{\mathbf{E}\cdot\boldsymbol{\tau}^2\}\{\boldsymbol{\phi}^*\cdot\boldsymbol{\tau}^2\}\,\mathrm{d}\boldsymbol{s},\\ B_S^{mm,1} &= \int_S(\chi_{mm}^{\boldsymbol{\tau}^1\boldsymbol{\tau}^1})^{-1}[\![\mathbf{E}\cdot\boldsymbol{\tau}^2]\!][\![\boldsymbol{\phi}^*\cdot\boldsymbol{\tau}^2]\!]\,\mathrm{d}\boldsymbol{s},\\ B_S^{mm,2} &= \int_S(\chi_{mm}^{\boldsymbol{\tau}^2\boldsymbol{\tau}^2})^{-1}[\![\mathbf{E}\cdot\boldsymbol{\tau}^1]\!][\![\boldsymbol{\phi}^*\cdot\boldsymbol{\tau}^1]\!]\,\mathrm{d}\boldsymbol{s}.\end{aligned}$$

The surfacic integrals in $B_S$ together with (E1) and additional boundary conditions at the edge of the simulation area to generate an input plane wave and to absorb all outgoing waves (open system) define the whole simulation problem.

## Appendix F: Additional details on numerical tests

### 1. Deflector

#### a. *Three-dimensional example*

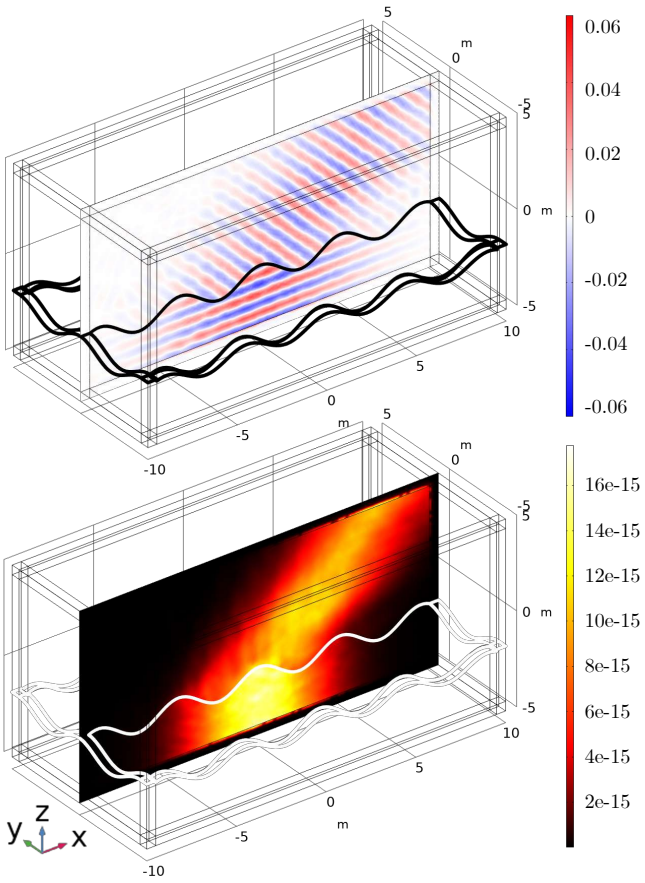


FIG. 5. Three-dimensional simulation of a sinusoidal light deflector using C-GSTCs. Top: real part of the $z$ component of the electric field. Bottom: energy density of the electromagnetic field.

In order to emphasize on the versatility of our FEM approach, we provide in Figure 5 the result of our simulation method on a three-dimensional sinusoidal metasurface. We considered here a $20\lambda \times 10\lambda \times 10\lambda$ simulation domain with a sinusoidal interface given by $f(x,y) = \frac{1}{2}\cos(\frac{4}{9}\pi x)\cos(\frac{4}{9}\pi y) - 2$ and an incident plane wave given by $\mathbf{E}_0(x,y,z) = (1,1,0)\exp(-ik_0 z)$.

#### b. *Sensitivity to the beam size*

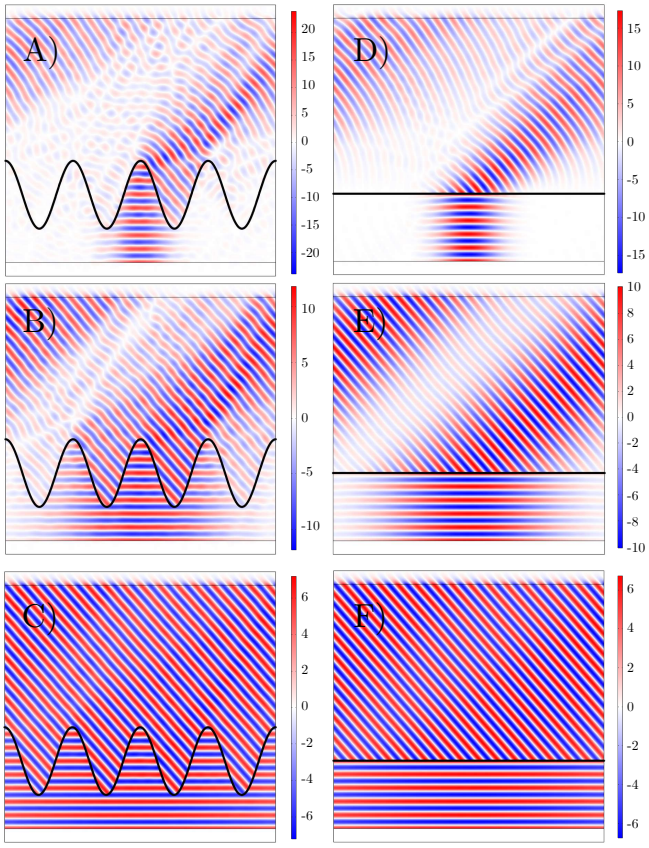


FIG. 6. Simulation of the sinusoidal (with sinusoids of amplitude $2.5\lambda$) and planar deflectors using an input Gaussian beam with varying variance $\sigma$. First column: conformal interface. Second column: planar interface. A)&D) $\sigma = 2\lambda$ B)&E) $\sigma = 6\lambda$, C)&F) $\sigma = 20\lambda$.

Another sensitivity analysis which was not studied in the main part of the paper is concerned with the beam size of the incident wave. Indeed, as we can see in Figure 2 C) and D), the susceptibilities associated with the planar surface have a period which is much smaller than the width of the simulation domain while the sinusoidal interface has susceptibilities which vary along the whole size of the periodic interface. This difference is important since sending an input wave beam with a radius smaller than the susceptibilities periodicity will inevitably degrade the solution. This can be seen in Figure 6 where Gaussian beams with different variances are considered.

### 2. Lens

#### a. *Three-dimensional example*

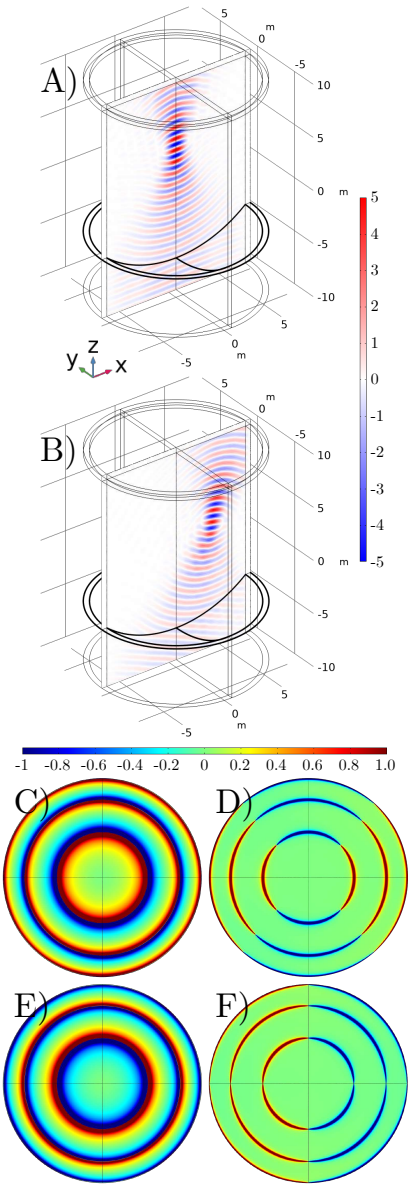


FIG. 7. Simulation of a three-dimensional curved metalens using C-GSTCs. A) Electric field (real part of $\mathbf{E}_z$) when the input wave is in the $z$ direction. B) Electric field for an input wave sent with an angle of 22.5 degrees with the $z$ axis. C)-F) Associated susceptibilities computed via the inversion procedure. C) real part of $\chi_{ee,0}^{\boldsymbol{\tau}^1\boldsymbol{\tau}^1}$ D) imaginary part of $\chi_{ee,0}^{\boldsymbol{\tau}^1\boldsymbol{\tau}^1}$ E) real part of $\chi_{mm,0}^{\boldsymbol{\tau}^2\boldsymbol{\tau}^2}$ D) imaginary part of $\chi_{mm,0}^{\boldsymbol{\tau}^2\boldsymbol{\tau}^2}$.

As in appendix F 1 a, we consider here the simulation of a three-dimensional metalens. The goal of this example is again only to show the application of our C-GSTCs to real three-dimensional structures. It is important to note that even if the simulation domain is invariant by rotation, it is still mandatory to perform a full three-dimensional simulation instead of an axisymmetric one since we are sending waves that are not always in the $z$ direction and thus are not invariant by rotation. Figure 7 shows the simulation result of the three-dimensional lens when a Gaussian wave is sent with two different angles.

Regarding the computation time, one simulation takes roughly 10 minutes on a 16 cores 3.2 GHz computing server with 200 gigabytes of dedicated memory. This has to be compared to the two-dimensional lenses considered in the main paper where one simulation only takes a couple of seconds on a common laptop.

### 3. Cloaking

#### a. *Synthesis using different internal fields*

We display in Figure 9 the reflected fields of the cloaking problem when considering different interior fields. These results have to be compared with the fields obtained for the mouse with the same angles. As it may be seen, even with $\pm 5$ degrees, the field reflected by the mouse shape is not really altered while depending on the considered interior field the illusion may not work when the incident angle is changed.

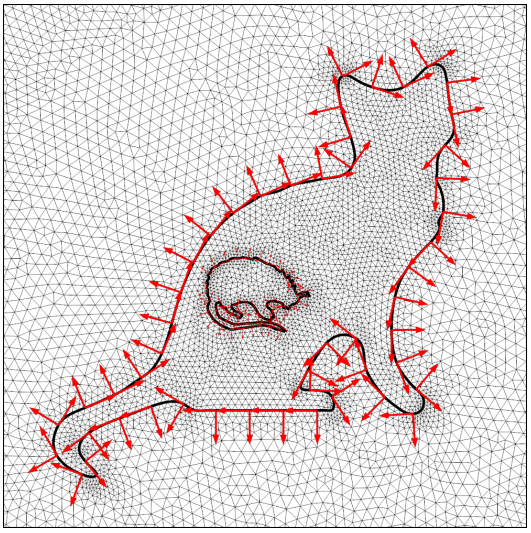

FIG. 8. Zoom on the mesh used for all the simulations of the cloaking system. The local basis vectors are represented in red along the cat and mouse interfaces.

We also show in Figure 8 the mesh which is used in the FEM simulations of the cloaking system. This figure clearly shows the benefit of using the FEM instead of the Finite Difference Time Domain (FDTD) method since a Cartesian grid, contrary to a triangular mesh, does not allow to handle such small geometric features and will inevitably lead to discrepancies in the results.

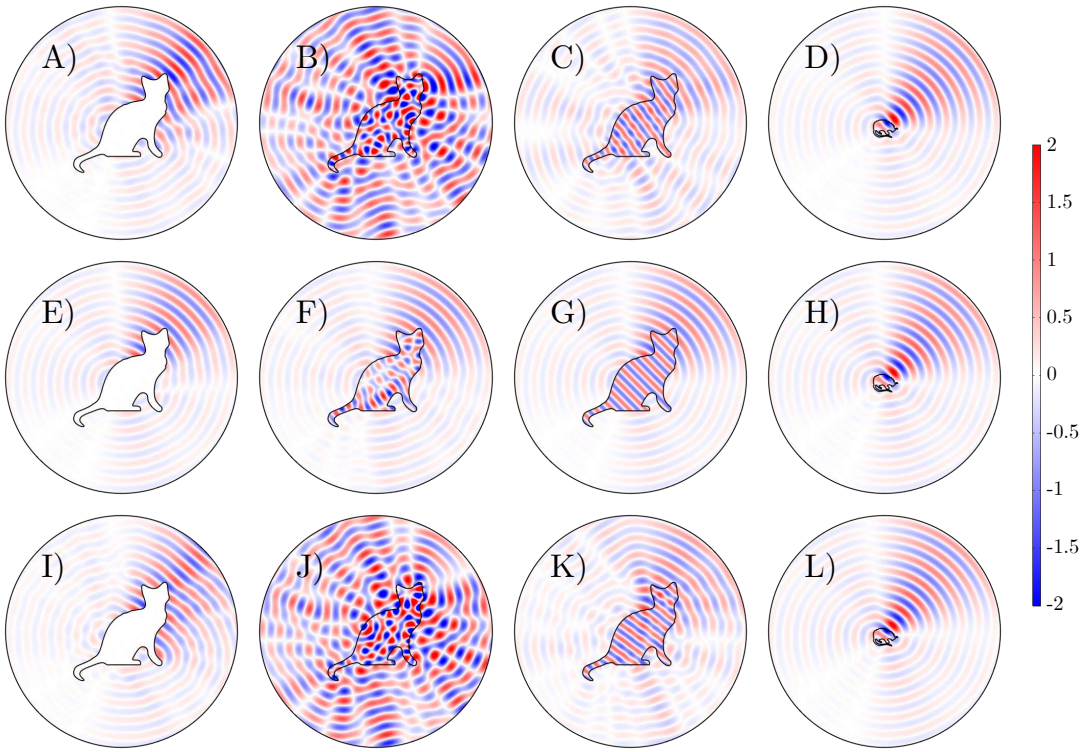


FIG. 9. Comparison of the reflected fields obtained using different interior field to synthesize the susceptibilities for the C-GSTCs to the reflected field of the classical shape used for the illusion. First row: angle of 40 degrees. Second row: angle of 45 degrees (C-GSTCs synthesized at this angle). Third row: angle of 50 degrees. First column: Synthesization using a zero interior field. Second column: Synthesization using an interior field equal to the one from the 'cat' simulation. Third column: Synthesization using a plane wave as interior field. Fourth column: Simulation of the reflected field by the 'mouse' shape.


[1] W. Cai, U. K. Chettiar, A. V. Kildishev, and V. M. Shalaev, Nature photonics **1**, 224 (2007).
[2] D. R. Smith, J. B. Pendry, and M. C. Wiltshire, Science **305**, 788 (2004).
[3] M. Scalora, G. D'Aguanno, N. Mattiucci, M. J. Bloemer, D. de Ceglia, M. Centini, A. Mandatori, C. Sibilia, N. Akozbek, M. G. Cappeddu, *et al.*, Optics Express **15**, 508 (2007).
[4] N. Yu, P. Genevet, M. A. Kats, F. Aieta, J.-P. Tetienne, F. Capasso, and Z. Gaburro, science **334**, 333 (2011).
[5] J. B. Pendry, D. Schurig, and D. R. Smith, science **312**, 1780 (2006).
[6] P. Genevet, F. Capasso, F. Aieta, M. Khorasaninejad, and R. Devlin, Optica **4**, 139 (2017).
[7] Q. Song, S. Khadir, S. Vézian, B. Damilano, P. Mierry, S. Chenot, V. Brandli, and P. Genevet, Science advances **7**, eabe1112 (2021).
[8] Q. Song, A. Baroni, R. Sawant, P. Ni, V. Brandli, S. Chenot, S. Vézian, B. Damilano, P. de Mierry, S. Khadir, *et al.*, Nature communications **11**, 1 (2020).
[9] V. A. Markel, JOSA A **33**, 1244 (2016).
[10] J. C. MAXWELL-GARNETT, Phil. Trans. R. Soc. Lond, A **203**, 385 (1904).
[11] P. A. Tirkas and K. R. Demarest, IEEE transactions on antennas and propagation **39**, 1338 (1991).
[12] J. G. Maloney and G. S. Smith, IEEE Transactions on Antennas and Propagation **41**, 690 (1993).
[13] M. Duruflé, V. Péron, and C. Poignard, Communications in Computational Physics **16**, 213 (2014).
[14] M. Idemen, Journal of the Physical Society of Japan **59**, 71 (1990).
[15] M. Dehmollaian and C. Caloz, in *2019 IEEE International Symposium on Antennas and Propagation and USNC-URSI Radio Science Meeting* (IEEE, 2019) pp. 1323–1324.
[16] Y. Zhang and Y. Tong, Optics Communications **483**, 126590 (2021).
[17] J. R. Ong, H. S. Chu, V. H. Chen, A. Y. Zhu, and P. Genevet, Optics letters **42**, 2639 (2017).
[18] T. Brown, C. Narendra, Y. Vahabzadeh, C. Caloz, and P. Mojabi, IEEE Transactions on Antennas and Propagation **68**, 1812 (2019).
[19] K. Achouri and C. Caloz, Nanophotonics **7**, 1095 (2018).
[20] K. Achouri, M. A. Salem, and C. Caloz, IEEE Transactions on Antennas and Propagation **63**, 2977–2991 (2015).
[21] S. Sandeep, J.-M. Jin, and C. Caloz, IEEE Transactions on Antennas and Propagation **65**, 2413 (2017).
[22] J.-M. Jin, *The finite element method in electromagnetics* (John Wiley & Sons, 2015).

[23] P. Monk *et al.*, *Finite element methods for Maxwell's equations* (Oxford University Press, 2003).
[24] Y. Vahabzadeh, K. Achouri, and C. Caloz, IEEE Transactions on Antennas and Propagation **64**, 4753 (2016).
[25] X. Jia, Y. Vahabzadeh, C. Caloz, and F. Yang, IEEE Transactions on Antennas and Propagation **67**, 2542 (2019).
[26] The Comsol models are attached as Supplementary Materials and will be freely available online once the reviewing process is over. These models allows for an easy simulation of any planar or conformal GSTCs with given susceptibilities (which can be found through the inversion procedure).
[27] C. Hockin, Journal of the Royal Microscopical Society **4**, 337 (1884).
[28] F. Aieta, P. Genevet, M. Kats, and F. Capasso, Optics express **21**, 31530 (2013).
[29] C. E. Gutiérrez, L. Pallucchini, and E. Stachura, JOSA A **34**, 1160 (2017).
[30] C. L. Holloway, E. F. Kuester, and A. Dienstfrey, Radio Science **49**, 813 (2014).
[31] N. Lebbe, K. Pham, and A. Maurel (2021), preprint available at https://hal.inria.fr/hal-03203013.
[32] K. Achouri, G. Lavigne, and C. Caloz, Journal of Applied Physics **120**, 235305 (2016).
[33] A. Henrot and M. Pierre, *Variation et optimisation de formes: une analyse géométrique*, Vol. 48 (Springer Science & Business Media, 2006).
[34] L. Onural, Journal of mathematical analysis and applications **322**, 18 (2006).
[35] M. M. Idemen, *Discontinuities in the electromagnetic field*, Vol. 40 (John Wiley & Sons, 2011).